Ultrastrong magnon-photon coupling, squeezed vacuum, and entanglement in superconductor/ferromagnet nanostructures

Mikhail Silaev[*]

Computational Physics Laboratory, Physics Unit, Faculty of Engineering and Natural Sciences,
Tampere University, P.O. Box 692, FI-33014, Tampere, Finland

Ultrastrong light-matter coupling opens exciting possibilities to generate squeezed quantum states and entanglement. We propose achieving this regime in superconducting hybrid nanostructures with ferromagnetic interlayers. Strong confinement of the electromagnetic field between superconducting plates results in the existence of magnon-polariton (MP) modes with ultrastrong magnon-photon coupling, ultrahigh cooperativity, and colossal group velocities. These modes provide a numerically accurate explanation of recent experiments and have intriguing quantum properties. The MP quantum vacuum consists of the squeezed magnon and photon states with the degree of squeezing controlled in wide limits by the external magnetic field. The ground-state population of virtual photons and magnons is vast and can be used for generating correlated magnon and photon pairs. MP excitations contain bipartite entanglement between magnons and photons. Our results indicate that superconducting/ferromagnet nanostructures are very promising for quantum magnonics.

Cavity-enhanced light-matter interaction has become one of the most prospective tools to control and study the properties of quantum materials [1–5]. At the core of this approach is the formation of hybrid quantum states consisting of matter and electromagnetic field components. This hybridization becomes especially pronounced in the strong-coupling regime when the coupling strength is larger than the decay rates of both the cavity and the quantum system states [6–10]. In many-body quantum systems, this regime leads to the formation of hybrid polaritons [3,11], combining photons and various collective modes. Among them are the exciton-polaritons [12], magnon-polaritons (MPs) [13,14], and hybrid superconducting modes [15–17].

Even more exciting is the ultrastrong coupling regime when the interaction is comparable with the eigenfrequencies of interacting modes [2,18]. In this regime, eigenstates combine many states with different numbers of particles, which can produce many exciting quantum effects. Given the rapidly developing field of quantum magnonics [13,14], it is very appealing to realize the ultrastrong-coupling regime in such systems where magnons represent matter, and the microwave cavity fields represent light. Previously, it has been achieved in specially designed three-dimensional (3D) microwave cavities [19] and in recently discovered on-chip superconducting nanostructures [20,21] combining superconducting (S) plates separated by the insulating (I) [22] and ferromagnetic metal (FM) interlayers typically of 10–100 nm thickness. The ultrastrong photon-magnon coupling observed in S/FM/I/S [20] and S/FM/S/I/S [21,23] systems is by several orders of magnitude larger than in S/FM [24,25] and S/FI bilayers [26],

where FI stands for a ferro- or ferrimagnetic insulator like yttrium iron garnet (YIG) [27,28].

In this letter, we explain these experiments by developing the theory of MP states for both the generic S/FI/S system and a more complex S/FM/I/S one which, however, has been studied experimentally [20]. Our theory is accurate in explaining these experiments [20] without adjusting parameters. In addition, we find several unique properties of MPs in such systems, making them a versatile platform for classical and quantum magnonics [27,29].

Let us consider the generic S/FI/S and S/FM/I/S systems, shown in Figs. 1(a) and 1(b), hosting both photonic modes and magnons. The former is represented by highly confined electromagnetic field solutions found by Swihart [22]. This Swihart mode is localized within the layer of the thickness $d_F + 2\lambda$ and $d_I + d_F + 2\lambda$ in S/FI/S and S/FM/I/S systems, respectively. Here, λ is the London penetration length in S. For typical superconducting material Nb [20,23] and nanostructure parameters $d_F, d_I \sim \lambda$, the field is localized within the layer much thinner than the photon wavelength, which is ~ 1–10 mm for microwave frequencies $\omega \sim 10$–100 GHz. This strong confinement leads to the unusual polarization structure with electric field $\mathbf{E}$ almost $\parallel \mathbf{q}$, as shown in Figs. 1(a) and 1(b) by blue arrows. Simultaneously, it leads to the strongly enhanced magnon-photon interaction as compared with the 3D cavities [13,14]. Dispersion of the Swihart mode is

$$\text{in S/FI/S:} \quad \Omega_{\text{Sw}}(q) = cq\sqrt{\frac{d_F}{\varepsilon(d_F + 2\lambda)}}, \tag{1}$$

$$\text{in S/FM/I/S:} \quad \Omega_{\text{Sw}}(q) = cq\sqrt{\frac{d_I}{\varepsilon(d_I + d_F + 2\lambda)}}, \tag{2}$$
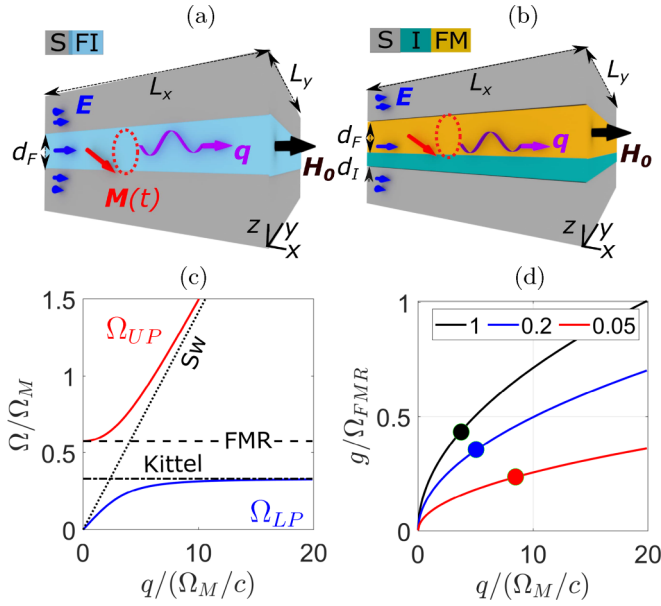
[*]silaev@kth.se

FIG. 1. Superconducting (S) structures hosting magnon-polariton (MP) modes with (a) a ferro- or ferrimagnetic insulator (FI) interlayer, (b) a composite interlayer consisting of a metallic ferromagnet (FM) and a usual insulator (I). The static external field is $\mathbf{H}_0 = H_0\mathbf{x}$, the precessing magnetization is $\mathbf{M}(t)$, and the wave vector of the MPs is $\mathbf{q} = q\mathbf{x}$. (c) MP spectrum in a S/FI/S system with $d_{\mathrm{FI}} = 0.3\lambda$. Upper Ω_{UP} and lower Ω_{LP} MPs are shown by red and blue lines, respectively. Dashed line is ferromagnetic resonance (FMR) frequency Ω_{FMR} in a S/FI/S system with $L_x = \infty$, dotted line is a Swihart (Sw) mode frequency Ω_{Sw}, dashed-dotted is the FMR Kittel frequency [30] in the isolated ferromagnetic film. Parameters are $d_F/\lambda = 0.5$, $H_0 = 4\pi M_0/10$, and $\Omega_M = 4\pi\gamma M_0$. (d) Coupling parameter $g(q)$ in Eq. (8) for $d_F/\lambda = 1$; 0.2; 0.05 and $H_0 = 4\pi M_0/10$. Filled circles show $g(q_{\mathrm{res}})$.

where c is light velocity, and $\varepsilon \sim 10$ is the dielectric constant in YIG or usual insulators Al_2O_3, Si.

Magnons in S/FI/S and S/FM/I/S systems are excitations of the magnetization direction $\mathbf{M}(t)$ in the magnetic layer. In thin films [20,31] $d_F \sim 100$ nm, the scale of magnon frequency dispersion [32–34] $q \sim d_F^{-1}$ is much larger than the wave numbers of microwave photons $q \sim 0.1$–1 mm^{-1}. Therefore, magnon frequency can be assumed constant, coinciding with the fundamental ferromagnetic resonance (FMR) mode Ω_{FMR}. In this regime, magnons play a role analogous to the electronic atomic [35] or intersubband transition in cavity electrodynamics [36]. The cavity is represented by the Swihart mode in Eqs. (1) and (2). The resonance when $\Omega_{\mathrm{Sw}}(q_{\mathrm{res}}) = \Omega_{\mathrm{FMR}}$ corresponds to the wavelengths $q_{\mathrm{res}}^{-1} \sim 1$–10 mm. The anticrossing between magnon and Swihart modes shown in Fig. 1(c) results in two MP modes. Detailed calculations yielding Fig. 1(c) are presented below.

Our starting equations for the frequency components of magnetization $\mathbf{M}_\omega$, magnetic field $\mathbf{H}_\omega$, and induction $\mathbf{B}_\omega = \mathbf{H}_\omega + 4\pi\mathbf{M}_\omega$ read

$$i\omega\mathbf{M}_\omega = \gamma(\mathbf{B}_0 \times \mathbf{M}_\omega + \mathbf{B}_\omega \times \mathbf{M}_0), \qquad (3)$$

$$\nabla \times (\tilde{\varepsilon}^{-1}\nabla \times \mathbf{H}_\omega) - q_v^2\mathbf{B}_\omega = 0. \qquad (4)$$

Here, Eq. (3) is the Landau-Lifshitz one, and $\mathbf{B}_0 = \mathbf{H}_0 + 4\pi\mathbf{M}_0$ is the stationary magnetic field. The gradient terms are neglected since length scales are much larger than the exchange length. The Maxwell equation result in Eq. (4) where $q_v = \omega/c$ is the wave number in vacuum. In the insulator, either FI or I, we have $\tilde{\varepsilon} = \varepsilon$, which is the dielectric constant, while in metal, $\tilde{\varepsilon} = -4\pi i\sigma/\omega$. The conductivity σ in FM is $\sigma_F = \mathrm{const.}$, while in S, $\sigma_S(\omega) = c^2/(4\pi i\lambda^2\omega)$, where λ is the London penetration length. We consider geometries in Figs. 1(a) and 1(b) such that $qL_y \ll 1$, corresponding to the experimental setups [20,21,23]. In this case, MP waves propagate only in the x direction, while along the y axis, all fields are homogeneous. Also, we assume that ferromagnetic films are thin $d_F \ll L_{x,y}$ which allows us to neglect stray fields.

First consider S/FI/S and S/FM/I/S systems shown in Figs. 1(a) and 1(b) with $L_x = \infty$ so that all fields perturbations $\propto e^{iqx}$ with arbitrary q. Time-dependent magnetization components are $\mathbf{M}_\omega = (0, M_{\omega y}, M_{\omega z})$. Due to the presence of metallic S layers, we can simplify the problem in the long-wavelength limit $q\lambda \ll 1$. In this case, Eq. (4) yields $B_{\omega z} = 0$ and $H_{\omega x} = 0$ in metallic S. Due to the continuity of $B_{\omega z}$ and $H_{\omega x}$, they are also small in the attached I and FI layers. Then we are left with equations only for the $H_{\omega y}$ component in each layer. Boundary conditions at interfaces follow directly from Maxwell equations, yielding the continuity of tangential components $H_{\omega y}$ and $E_{\omega x}$, where $E_{\omega x} = (i/\tilde{\varepsilon}q_v)\nabla_z H_{\omega y}$.

Solving equations for $H_{\omega y}$ in different domains and matching them with the help of the above boundary conditions [37], we get the MP dispersion relation which looks similar for both S/FI/S and S/FM/I/S systems:

$$(\omega^2 - \Omega_{\mathrm{Sw}}^2)(\omega^2 - \Omega_{\mathrm{FMR}}^2) = 4g^2\Omega_{\mathrm{FMR}}\Omega_{\mathrm{Sw}}. \qquad (5)$$

Here, $\Omega_{\mathrm{Sw}}(q)$ is the Swihart mode frequency in Eqs. (1) and (2), and Ω_{FMR} is the FMR frequency given by

$$\text{in S/FI/S:} \quad \Omega_{\mathrm{FMR}} = \gamma\sqrt{H_0 B_0 + \frac{4\pi M_0 B_0 d_F}{d_F + 2\lambda}}, \qquad (6)$$

$$\text{in S/FM/I/S:} \quad \Omega_{\mathrm{FMR}} = \gamma\sqrt{H_0 B_0 + \frac{4\pi M_0 B_0 d_F}{d_I + d_F + 2\lambda}}. \qquad (7)$$

Both Eqs. (6) and (7) demonstrate the detuning from the FMR frequency in isolated ferromagnetic film derived by Kittel [30] $\Omega_K = \gamma\sqrt{H_0 B_0}$. The magnon-photon coupling parameter in Eq. (5) equivalent to the vacuum Rabi splitting [1,35,36,38] is

$$g = \frac{1}{2}\sqrt{\frac{\Omega_{Sw}}{\Omega_{\mathrm{FMR}}}}\sqrt{\Omega_{\mathrm{FMR}}^2 - \Omega_K^2}. \qquad (8)$$

The solution of Eq. (5) consists of upper and lower MP modes with frequencies $\Omega_{\mathrm{UP}}(q)$ and $\Omega_{\mathrm{LP}}(q)$, respectively, where $\Omega_{\mathrm{UP}} > \Omega_{\mathrm{LP}}$. The example of dispersion curves for the S/FI/S system with $d_F = 0.5\lambda$ is shown in Fig. 1(c). The coupling parameter in Eq. (8) is determined by the detuning $g \propto \sqrt{\Omega_{\mathrm{FMR}}^2 - \Omega_K^2}$ which strongly depends on thickness d_F and external parameters such as H_0 and temperature T through the London length $\lambda(T)$. Shown in Fig. 1(b) are the dependencies $g(q)$ in S/FI/S for $d_F/\lambda = 1; 0.2; 0.05$. As one can see, it is possible to achieve an ultrastrong photon-magnon coupling when $g \sim \Omega_{\mathrm{FMR}}$ [2,36]. Indeed, at resonant

point [36] q_{res}, where $\Omega_{\mathrm{Sw}}(q_{\mathrm{res}}) = \Omega_{\mathrm{FMR}}$, the coupling parameter is $g(q_{\mathrm{res}}) = \gamma \sqrt{\pi B_0 M_0 d_F / (d_F + 2\lambda)}$. The maximal value $g(q_{\mathrm{res}}) = \Omega_{\mathrm{FMR}}/2$ is reached at $H_0 = 0$. Due to this upper boundary, it is not possible to achieve a deep-strong-coupling [39–41] regime and a superradiant transition. A similar result is valid for the S/FM/I/S system.

The dispersion relation in Eq. (5) can be written in the form introduced to fit the experimental data [20], which follows from the Hopfield Hamiltonian [2,40,42,43]:

$$\omega^4 - \omega^2\left(\Omega_{\mathrm{Sw}}^2 + \Omega_K^2 + 4\tilde{g}^2\right) + \Omega_{\mathrm{Sw}}\Omega_K = 0. \quad (9)$$

Here, the renormalized coupling $\tilde{g} = \sqrt{\Omega_{\mathrm{FMR}}^2 - \Omega_K^2}$ is

$$\text{in S/FI/S:} \quad \tilde{g} = \gamma \sqrt{\frac{\pi M_0 B_0 d_F}{(d_F + 2\lambda)}}, \quad (10)$$

$$\text{in S/FM/I/S:} \quad \tilde{g} = \gamma \sqrt{\frac{\pi M_0 B_0 d_F}{(d_F + d_I + 2\lambda)}}. \quad (11)$$

For small external fields $H_0 \ll 4\pi M_0$, the coupling coefficient is almost constant at $\tilde{g}(H_0) \approx \mathrm{const}$. As shown in Ref. [20], this allows obtaining accurate fits of experimental data using Eq. (9) with $\tilde{g}$ as a phenomenological parameter.

Both S/FI/S and S/FM/I/S systems provide ultrahigh cooperativity for MP states. The cooperativity is $C = g(q_{\mathrm{res}})/(\alpha_{\mathrm{ph}}\alpha_{\mathrm{mag}})$, where α_{ph} and α_{mag} are the photon and magnon decay rates, respectively. For the S/FI/S system with YIG, we assume [26] $\alpha_{\mathrm{ph}} = 3\,\mathrm{MHz}$, $\alpha_{\mathrm{mag}} = 50\,\mathrm{MHz}$, and $\Omega_M \approx 6\,\mathrm{GHz}$. For parameters corresponding to Fig. 1(c), Eqs. (6) and (8) yield $C = 1.3 \times 10^4$. A similar estimation can be made for the S/FM/I/S system with Py ferromagnet and parameters corresponding to experiment [20] $d_I = d_F = 0.3\lambda$. Assuming that the decay rates are [25] $\alpha_{\mathrm{ph}} = 0.7\,\mathrm{MHz}$, $\alpha_{\mathrm{mag}} = 200\,\mathrm{MHz}$, and $\Omega_M = 31.3\,\mathrm{GHz}$ and $H_0 = 4\pi M_0/10$, from Eqs. (8) and (7), we get $C = 3.7 \times 10^5$. This ultrahigh cooperativity is comparable with the one achieved in the specially designed 3D cavities with focused magnetic fields [44].

In the region of strong magnon-photon mixing $q \approx q_{\mathrm{res}}$ in Fig. 1(c), the group velocities of MP branches $v_j = \partial\Omega_j/\partial q$ are of the order $v_j \sim c/20 \approx 1.5 \times 10^4\,\mathrm{km/s}$. This velocity is 10^4 times larger than that of the fastest known magnons [45]. In complement to magnon gating by narrow S stripes [46] and magnon-condensate coupling [47], the present S/FI/S and S/FM/I/S systems are extremely efficient in transmitting magnetic signals which is promising for ultrafast and energy-efficient data processing [29]. Realization of such propagating MPs in experiments requires samples with length $L_x \gg 1/q_{\mathrm{res}}$ which in existing S/FM/I/S structures means [20,21,23] $L_x \sim 1\,\mathrm{cm}$. Larger q_{res} and smaller L_x can be achieved by reducing the Swihart mode velocity in Eq. (1), increasing λ, or reducing the S layer thickness [22].

In several limiting cases, MPs feature interesting behavior. (i) For $H_0 = 0$, Eq. (8) yields $g = \sqrt{\Omega_{\mathrm{Sw}}\Omega_{\mathrm{FMR}}}/2$ so that $\Omega_{\mathrm{LP}}(H_0 = 0) = 0$ and $\Omega_{\mathrm{UP}}(H_0 = 0) = \sqrt{\Omega_{\mathrm{Sw}}^2 + \Omega_{\mathrm{FMR}}^2}$. The asymptotic behavior for small fields $H_0 \ll M_0$ is $\Omega_{\mathrm{LP}} = \Omega_K\Omega_{\mathrm{Sw}}/\sqrt{\Omega_{\mathrm{Sw}}^2 + \Omega_{\mathrm{FMR}}^2} \propto \gamma\sqrt{H_0 M_0}$. As shown below, this behavior is crucial for realizing highly squeezed vacuum magnon and photon states. (ii) For large wave numbers $q \gg \Omega_M/c$, the asymptote is $\Omega_{\mathrm{UP}}(q \to \infty) = \Omega_{\mathrm{Sw}}$ and $\Omega_{\mathrm{LP}}(q \to$
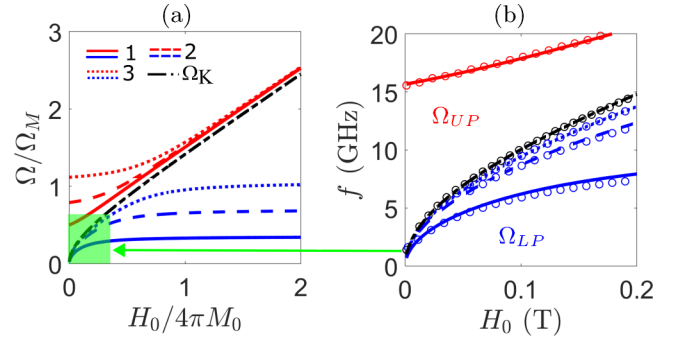

FIG. 2. (a) Quantized magnon-polariton (MP) modes in a S/FM/I/S system with parameters as in experiment [20], see text for details. Upper (red lines) $\Omega_{\mathrm{UP},n}(H_0)$ and lower (blue lines) $\Omega_{\mathrm{LP},n}(H_0)$ modes with $n = 1$ (solid lines), $n = 2$ (dashed lines), and $n = 3$ (dotted lines). The black dash-dotted line is the Kittel frequency $\Omega_K(H_0)$ of ferromagnetic resonance (FMR) in an isolated ferromagnetic film. (b) The zoomed-in region marked by green rectangle in (a) plotted in real units. Open circles show experimental data [20].

$\infty) = \Omega_K$, as can be seen in Fig. 1(c). This behavior explains earlier theoretical results [48] and experiments [49] in S/FM/I/S systems much shorter than the wavelength $L_x \ll c/\Omega_M$, showing that the measured FMR frequency is equal to that of the isolated FM film Ω_K. As discussed below, the standing waves of MPs have quantized wave numbers $q_n = \pi n/L_x$ with integer $n > 0$. For small L_x, all such wave numbers are high $q_n \gg q_{\mathrm{res}}$ so that the corresponding lower MP frequencies observed in FMR experiments [49] are identical $\Omega_{\mathrm{LP}}(q_n) \approx \Omega_K$. (iii) For $d_I \to 0$, the Swihart mode velocity in Eq. (2) in the S/FM/I/S system becomes very small. Then according to Fig. 1(c), the lower MP mode disappears $\Omega_{\mathrm{LP}}(q) \to 0$. At the same time, the upper MP mode becomes dispersionless $\Omega_{\mathrm{UP}}(q) \approx \Omega_{\mathrm{FMR}}$, given by Eq. (7) with $d_I = 0$. This result coincides with previous calculations [48] and shows that experiments [49–51] in S/FM/S systems have measured in fact the upper MP modes, having $\Omega_{\mathrm{UP}}(q_n) \approx \Omega_{\mathrm{FMR}}$ for all integer n.

The quantization of MP states was observed in recent experiments [20,23]. To apply our theory, we note that structures of finite length L_x, shown in Figs. 1(a) and 1(b), host standing waves of MPs with discrete momenta $q_n = \pi n/L_x$ with integer $n > 0$. The corresponding discrete frequencies $\Omega_{\mathrm{LP},n}$ and $\Omega_{\mathrm{UP},n}$ are given directly by Eq. (5) with $q = q_n$; that is $\Omega_{j,n} = \Omega_j(q_n)$, where $j = \{\mathrm{LP}, \mathrm{UP}\}$. Let us consider the S/FM/I/S structure shown in Fig. 1(b) with parameters precisely those used in experiment [20]: $\lambda = 80\,\mathrm{nm}$, $d_F = 25\,\mathrm{nm}$, $d_I = 13\,\mathrm{nm}$, $L_x = 1.1\,\mathrm{mm}$, $\varepsilon = 10$, and $M_0 = 1.06\,\mathrm{T}$, so that $\Omega_M = 31.3\,\mathrm{GHz}$. In Figs. 2(a) and 2(b), the blue and red lines show $\Omega_{\mathrm{LP},n}(H_0)$ and $\Omega_{\mathrm{UP},n}(H_0)$, respectively, for $n = 1, 2, 3$. As shown in Fig. 2, the sequence of modes $\Omega_{\mathrm{LP},n}(H_0)$ is limited from above by the Kittel frequency since, as discussed above, $\Omega_{\mathrm{LP}}(q \to \infty) = \Omega_K$. The other sequence $\Omega_{\mathrm{UP},n}(H_0)$ grows unbounded with n. To compare with experiment [20], we consider the domain marked by the green rectangle in Fig. 2(a) and plot it in physical units in Fig. 2(b). There is very accurate agreement between experimental data [20] shown by open circles and theory curves shown by solid lines. Note that we use no adjusting parameters. Qualitatively similar results
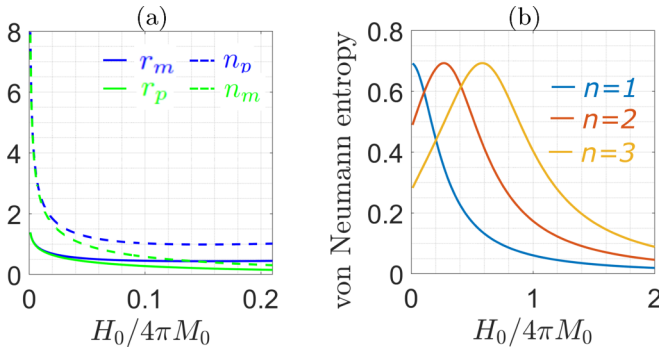
FIG. 3. (a) Magnon r_m and photon r_p squeeze parameters for the vacuum state of lower magnon-polariton (MP) mode with $n = 1$ in a S/FM/I/S system. (b) von Neumann entropy measuring the photon-magnon entanglement in the excited states of lower MP mode with $n = 1$; 2; 3 in a S/FM/I/S system. Parameters are the same as in Fig. 2(b).

are given by Eqs. (1), (5), and (6) for the S/FI/S system in Fig. 1(b), which is yet to be realized experimentally.

The dispersion relation in Eqs. (5) and (7) does not consider the presence of Abrikosov vortices in S layers [52–54] generated by the external field $\mathbf{H}_0 \parallel \mathbf{x}$. Since currents generated by MP field $H_{\omega y}\mathbf{y}$ in S layers flow in the x direction, such vortices do not move. Vortices affect the MP frequencies by suppressing the order parameter and increasing the effective London length. However, at fields up to $H_0 = 0.2$ T, as in Fig. 2(b), such a frequency correction is not larger than 1–2%.

The MP dispersion relation in Eq. (5) is equivalent to the Dicke-model Hamiltonian [36,55–58]:

$$\hat{H} = \Omega_{\mathrm{Sw}}\hat{a}^\dagger\hat{a} + \Omega_{\mathrm{FMR}}\hat{b}^\dagger\hat{b} + g(\hat{a} + \hat{a}^\dagger)(\hat{b}^\dagger + \hat{b}), \quad (12)$$

where $\hat{a}$ and $\hat{b}$ are the annihilation operators for the photon and magnon modes with quantum number n. The photon frequency and coupling are given by Eq. (5) with $\Omega_{\mathrm{Sw}} = \Omega_{\mathrm{Sw}}(q_n)$ and $g = g(q_n)$. The last term in Eq. (12) is the quantized Zeeman interaction energy [37] $d_F H_y M_y$.

The Hamiltonian in Eq. (12) is diagonalized in terms of the MP operators $\hat{d}_j^\dagger = p_j\hat{a}^\dagger + m_j\hat{b}^\dagger + \tilde{p}_j\hat{a} + \tilde{m}_j\hat{b}$, where $j = \{\mathrm{UP}, \mathrm{LP}\}$. Coefficients of mixing fractions can be chosen as real and satisfy the normalization condition $p_j^2 + m_j^2 - \tilde{p}_j^2 - \tilde{m}_j^2 = 1$. Their behavior is shown as a function of H_0 in Fig. 3(a) for the lower MP branch with $n = 1$. Squeezed vacuum states [59,60] $|0\rangle_{\mathrm{sq}}$ are defined separately for every quantized mode as $\hat{d}_j|0\rangle_{\mathrm{sq}} = 0$. Annihilation operators for each n can be written as $\hat{d}_{\mathrm{LP}} = \hat{S}_p\hat{S}_m(\alpha\hat{a} + \beta\hat{b})\hat{S}_p^\dagger S_m^\dagger$ using magnon $\hat{S}_m = \exp[r_m(\hat{b}^2 - \hat{b}^{\dagger 2})/2]$ and photon $\hat{S}_p = \exp[r_p(\hat{a}^2 - \hat{a}^{\dagger 2})/2]$ squeezing operators [37,59,60]. Here, the squeezing parameters are $r_p = \mathrm{atanh}(\tilde{p}_{\mathrm{LP}}/p_{\mathrm{LP}})$ and $r_m = \mathrm{atanh}(\tilde{m}_{\mathrm{LP}}/m_{\mathrm{LP}})$. The vacuum state is obtained by squeezing both photons and magnons $|0\rangle_{\mathrm{sq}} = \hat{S}_p\hat{S}_m|0, 0\rangle$, where $|0, 0\rangle$ is the usual vacuum state. As shown in Fig. 3(a), squeeze parameters strongly depend on H_0. For $H_0 \ll M_0$, we get $r_p = \Omega_{\mathrm{UP}}/2\Omega_K$ and $r_m = (\Omega_{\mathrm{FMR}}/\Omega_{\mathrm{Sw}})\Omega_{\mathrm{UP}}/2\Omega_K$; that

is divergence $r_{m,p} \sim \sqrt{M_0/H_0}$. Hence, in the limit $H_0 \to 0$, such squeezing can become quite large compared with the highest known photon squeezing with [61,62] $r_p = 1.7$ and even sublattice magnon squeezing $r_m \sim 3$ in antiferromagnets [63]. It can be used for quantum sensing applications [64] and generation of nonclassical photon [61] and magnon states [65,66].

Squeezed vacuum states are characterized by the nonzero density of virtual excitations [2,36,67]. The populations of virtual photons and magnons are $n_p = \langle 0|\hat{a}^\dagger\hat{a}|0\rangle_{\mathrm{sq}} = \sinh(2r_p)$ and $n_m = \langle 0|\hat{b}^\dagger\hat{b}|0\rangle_{\mathrm{sq}} = \sinh(2r_m)$, respectively. At $H_0 \ll 4\pi M_0$, populations diverge exponentially, as shown in Fig. 3(a). This effect is very promising for generating entangled photon and magnon pairs through the analog of the dynamical Casimir effect involving abrupt changes of vacuum state populations [2,36,67–75]. Photon and magnon pairs can be effectively generated [36] by varying H_0 or λ faster than the MP frequencies $\Omega_{\mathrm{LP},n}$.

Finally, let us demonstrate the magnon-photon entanglement which has attracted a lot of attention recently [76–78]. Due to the ultrastrong magnon-photon coupling, entanglement can be obtained in our on-chip systems, Figs. 1(a) and 1(b), without extra complicated conditions. In contrast, the generation of magnon-photon entanglement in systems with weaker beam-splitter-type couplings requires either nonlinear magnetoelastic interaction [77] or non-Hermitian $\mathcal{PT}$-symmetry breaking [78]. Acting with the lower MP creation operator on the corresponding vacuum state, we get the excited state given by $|1\rangle = \hat{d}_{\mathrm{LP}}^\dagger|0\rangle_{\mathrm{sq}}$. This state consists [37] of nonseparable magnon and photon parts. Their entanglement is determined by the von Neumann entropy [59,79] $S_{mp} = -\mathrm{Tr}(\hat{\rho}_p \ln \hat{\rho}_p)$. Here, the reduced density matrix is calculated taking the trace over magnon states $\hat{\rho}_p = \mathrm{Tr}_m\langle\psi_m|\hat{\rho}|\psi_m\rangle$ from the full density matrix corresponding to the pure excited MP state, which is $\hat{\rho} = |1\rangle\langle 1|$. The resulting dependencies of $S_{mp}(H_0)$ for the lower MP modes with $n = 1$; 2; 3 are shown in Fig. 3(b) for the S/FM/I/S system with parameters the same as in Fig. 2(b) and experiment [20]. Such a high von Neumann entropy $S_{mp} \sim 1$ which has been measured before only in cold atomic systems [80] can have many practical applications, transferring entanglement between different types of quantum systems.

To summarize, we have found a mechanism of ultrastrong magnon-photon coupling in superconductor/ferromagnet nanostructures. This coupling produces highly squeezed vacuum states with many virtual photons and magnons at microwave frequencies. Our theory yields MP modes with ultrahigh cooperativity propagating with the velocity of $\sim 10^4$ km/s. Calculated MP frequency spectra accurately explain recent experiments. Excited MP states consist of entangled magnon and photon states with large bipartite von Neumann entropy. These exciting properties put forward the suggested superconductor/ferromagnet nanostructures as promising platforms for various classical and quantum magnonics applications.

[1] J.-M. Raimond, M. Brune, and S. Haroche, Rev. Mod. Phys. **73**, 565 (2001).

[2] A. Frisk Kockum, A. Miranowicz, S. De Liberato, S. Savasta, and F. Nori, Nat. Rev. Phys. **1**, 19 (2019).

[3] D. Basov, R. Averitt, and D. Hsieh, Nat. Mater. **16**, 1077 (2017).

[4] J. Bloch, A. Cavalleri, V. Galitski, M. Hafezi, and A. Rubio, Nature (London) **606**, 41 (2022).

[5] F. Schlawin, D. M. Kennes, and M. A. Sentef, Appl. Phys. Rev. **9**, 011312 (2022).

[6] Y. Kaluzny, P. Goy, M. Gross, J. M. Raimond, and S. Haroche, Phys. Rev. Lett. **51**, 1175 (1983).

[7] D. Meschede, H. Walther, and G. Müller, Phys. Rev. Lett. **54**, 551 (1985).

[8] R. J. Thompson, G. Rempe, and H. J. Kimble, Phys. Rev. Lett. **68**, 1132 (1992).

[9] P. Lodahl, S. Mahmoodian, and S. Stobbe, Rev. Mod. Phys. **87**, 347 (2015).

[10] X. Gu, A. F. Kockum, A. Miranowicz, Y.-x. Liu, and F. Nori, Phys. Rep. **718-719**, 1 (2017).

[11] D. Basov, M. Fogler, and F. García de Abajo, Science **354**, aag1992 (2016).

[12] H. Deng, H. Haug, and Y. Yamamoto, Rev. Mod. Phys. **82**, 1489 (2010).

[13] D. Lachance-Quirion, Y. Tabuchi, A. Gloppe, K. Usami, and Y. Nakamura, Appl. Phys. Express **12**, 070101 (2019).

[14] B. Z. Rameshti, S. V. Kusminskiy, J. A. Haigh, K. Usami, D. Lachance-Quirion, Y. Nakamura, C.-M. Hu, H. X. Tang, G. E. Bauer, and Y. M. Blanter, Phys. Rep. **979**, 1 (2022).

[15] A. A. Allocca, Z. M. Raines, J. B. Curtis, and V. M. Galitski, Phys. Rev. B **99**, 020504(R) (2019).

[16] J. B. Curtis, Z. M. Raines, A. A. Allocca, M. Hafezi, and V. M. Galitski, Phys. Rev. Lett. **122**, 167002 (2019).

[17] J. B. Curtis, A. Grankin, N. R. Poniatowski, V. M. Galitski, P. Narang, and E. Demler, Phys. Rev. Res. **4**, 013101 (2022).

[18] P. Forn-Díaz, L. Lamata, E. Rico, J. Kono, and E. Solano, Rev. Mod. Phys. **91**, 025005 (2019).

[19] N. Kostylev, M. Goryachev, and M. E. Tobar, Appl. Phys. Lett. **108**, 062402 (2016).

[20] I. A. Golovchanskiy, N. N. Abramov, V. S. Stolyarov, A. A. Golubov, M. Y. Kupriyanov, V. V. Ryazanov, and A. V. Ustinov, Phys. Rev. Appl. **16**, 034029 (2021).

[21] I. A. Golovchanskiy, N. N. Abramov, V. S. Stolyarov, P. S. Dzhumaev, O. V. Emelyanova, A. A. Golubov, V. V. Ryazanov, and A. V. Ustinov, Adv. Sci. **6**, 1900435 (2019).

[22] J. C. Swihart, J. Appl. Phys. **32**, 461 (1961).

[23] I. A. Golovchanskiy, N. N. Abramov, V. S. Stolyarov, M. Weides, V. V. Ryazanov, A. A. Golubov, A. V. Ustinov, and M. Y. Kupriyanov, Sci. Adv. **7**, eabe8638 (2021).

[24] Y. Li, T. Polakovic, Y.-L. Wang, J. Xu, S. Lendinez, Z. Zhang, J. Ding, T. Khaire, H. Saglam, R. Divan et al., Phys. Rev. Lett. **123**, 107701 (2019).

[25] J. T. Hou and L. Liu, Phys. Rev. Lett. **123**, 107702 (2019).

[26] H. Huebl, C. W. Zollitsch, J. Lotze, F. Hocke, M. Greifenstein, A. Marx, R. Gross, and S. T. B. Goennenwein, Phys. Rev. Lett. **111**, 127003 (2013).

[27] A. Chumak, V. Vasyuchka, A. Serga, and B. Hillebrands, Nat. Phys. **11**, 453 (2015).

[28] A. Serga, A. Chumak, and B. Hillebrands, J. Phys. D **43**, 264002 (2010).

[29] A. V. Chumak, P. Kabos, M. Wu, C. Abert, C. Adelmann, A. O. Adeyeye, J. Åkerman, F. G. Aliev, A. Anane, A. Awad et al., IEEE Trans. Magn. **58**, 0800172 (2022).

[30] C. Kittel, Phys. Rev. **73**, 155 (1948).

[31] M. Schneider, D. Breitbach, R. O. Serha, Q. Wang, A. A. Serga, A. N. Slavin, V. S. Tiberkevich, B. Heinz, B. Lägel, T. Brächer et al., Phys. Rev. Lett. **127**, 237203 (2021).

[32] R. W. Damon and J. Eshbach, J. Phys. Chem. Solids **19**, 308 (1961).

[33] B. Kalinikos, in IEE Proceedings H (Microwaves, Optics and Antennas), Vol. 127 (IET, 1980), pp. 4–10.

[34] A. Prabhakar and D. D. Stancil, Spin Waves: Theory and Applications, Vol. 5 (Springer, New York, 2009).

[35] G. Rempe, H. Walther, and N. Klein, Phys. Rev. Lett. **58**, 353 (1987).

[36] C. Ciuti, G. Bastard, and I. Carusotto, Phys. Rev. B **72**, 115303 (2005).

[37] See Supplemental Material at http://link.aps.org/supplemental/10.1103/PhysRevB.107.L180503 for technical calculation details of the MP spectrum in S/FI/S and S/FM/I/S systems as well as the structure of squeezed vacuum state and magnon-photon entanglement.

[38] C. Weisbuch, M. Nishioka, A. Ishikawa, and Y. Arakawa, Phys. Rev. Lett. **69**, 3314 (1992).

[39] J. Casanova, G. Romero, I. Lizuain, J. J. García-Ripoll, and E. Solano, Phys. Rev. Lett. **105**, 263603 (2010).

[40] A. Bayer, M. Pozimski, S. Schambeck, D. Schuh, R. Huber, D. Bougeard, and C. Lange, Nano Lett. **17**, 6340 (2017).

[41] F. Yoshihara, T. Fuse, S. Ashhab, K. Kakuyanagi, S. Saito, and K. Semba, Nat. Phys. **13**, 44 (2017).

[42] D. G. Baranov, B. Munkhbat, E. Zhukova, A. Bisht, A. Canales, B. Rousseaux, G. Johansson, T. J. Antosiewicz, and T. Shegai, Nat. Commun. **11**, 2715 (2020).

[43] N. S. Mueller, Y. Okamura, B. G. Vieira, S. Juergensen, H. Lange, E. B. Barros, F. Schulz, and S. Reich, Nature (London) **583**, 780 (2020).

[44] M. Goryachev, W. G. Farr, D. L. Creedon, Y. Fan, M. Kostylev, and M. E. Tobar, Phys. Rev. Appl. **2**, 054002 (2014).

[45] Y.-J. Chen, K. Zakeri, A. Ernst, H. J. Qin, Y. Meng, and J. Kirschner, Phys. Rev. Lett. **119**, 267201 (2017).

[46] T. Yu and G. E. W. Bauer, Phys. Rev. Lett. **129**, 117201 (2022).

[47] L. G. Johnsen, H. T. Simensen, A. Brataas, and J. Linder, Phys. Rev. Lett. **127**, 207001 (2021).

[48] M. Silaev, Phys. Rev. Appl. **18**, L061004 (2022).

[49] L.-L. Li, Y.-L. Zhao, X.-X. Zhang, and Y. Sun, Chin. Phys. Lett. **35**, 077401 (2018).

[50] K.-R. Jeon, C. Ciccarelli, H. Kurebayashi, L. F. Cohen, X. Montiel, M. Eschrig, T. Wagner, S. Komori, A. Srivastava, J. W. A. Robinson et al., Phys. Rev. Appl. **11**, 014061 (2019).

[51] I. A. Golovchanskiy, N. N. Abramov, V. S. Stolyarov, V. I. Chichkov, M. Silaev, I. V. Shchetinin, A. A. Golubov, V. V. Ryazanov, A. V. Ustinov, and M. Y. Kupriyanov, Phys. Rev. Appl. **14**, 024086 (2020).

[52] S. H. Brongersma, E. Verweij, N. J. Koeman, D. G. De Groot, R. Griessen, and B. I. Ivlev, Phys. Rev. Lett. **71**, 2319 (1993).

[53] D. Luzhbin, Phys. Solid State **43**, 1823 (2001).

[54] V. K. Vlasko-Vlasov, F. Colauto, A. A. Buzdin, D. Carmo, A. M. H. Andrade, A. A. M. Oliveira, W. A. Ortiz, D. Rosenmann, and W.-K. Kwok, Phys. Rev. B **94**, 184502 (2016).

[55] R. H. Dicke, Phys. Rev. **93**, 99 (1954).

[56] J. Hopfield, Phys. Rev. **112**, 1555 (1958).

[57] K. Hepp and E. H. Lieb, Ann. Phys. **76**, 360 (1973).

[58] C. Emary and T. Brandes, Phys. Rev. E **67**, 066203 (2003).

[59] C. Gerry, P. Knight, and P. L. Knight, *Introductory Quantum Optics* (Cambridge University Press, Cambridge, 2005).

[60] A. B. Klimov and S. M. Chumakov, *A Group-Theoretical Approach to Quantum Optics: Models of Atom-Field Interactions* (WILEY-VCH Verlag GmbH & Co. KGaA, Weinheim, 2009).

[61] R. Schnabel, Phys. Rep. **684**, 1 (2017).

[62] H. Vahlbruch, M. Mehmet, K. Danzmann, and R. Schnabel, Phys. Rev. Lett. **117**, 110801 (2016).

[63] A. Kamra, E. Thingstad, G. Rastelli, R. A. Duine, A. Brataas, W. Belzig, and A. Sudbø, Phys. Rev. B **100**, 174407 (2019).

[64] C. L. Degen, F. Reinhard, and P. Cappellaro, Rev. Mod. Phys. **89**, 035002 (2017).

[65] A. Kamra and W. Belzig, Phys. Rev. Lett. **116**, 146601 (2016).

[66] S. A. Bender, A. Kamra, W. Belzig, and R. A. Duine, Phys. Rev. Lett. **122**, 187701 (2019).

[67] S. De Liberato, Nat. Commun. **8**, 1465 (2017).

[68] P. Lähteenmäki, G. S. Paraoanu, J. Hassel, and P. J. Hakonen, Nat. Commun. **7**, 12548 (2016).

[69] P. Lähteenmäki, G. Paraoanu, J. Hassel, and P. J. Hakonen, Proc. Natl. Acad. Sci. **110**, 4234 (2013).

[70] G. T. Moore, J. Math. Phys. **11**, 2679 (1970).

[71] P. D. Nation, J. R. Johansson, M. P. Blencowe, and F. Nori, Rev. Mod. Phys. **84**, 1 (2012).

[72] G. S. Paraoanu and G. Johansson, Europhysics News **51**, 18 (2020).

[73] C. M. Wilson, G. Johansson, A. Pourkabirian, M. Simoen, J. R. Johansson, T. Duty, F. Nori, and P. Delsing, Nature (London) **479**, 376 (2011).

[74] J. R. Johansson, G. Johansson, C. M. Wilson, and F. Nori, Phys. Rev. A **82**, 052509 (2010).

[75] J. R. Johansson, G. Johansson, C. M. Wilson, and F. Nori, Phys. Rev. Lett. **103**, 147003 (2009).

[76] H. Yuan, Y. Cao, A. Kamra, R. A. Duine, and P. Yan, Phys. Rep. **965**, 1 (2022).

[77] J. Li, S.-Y. Zhu, and G. S. Agarwal, Phys. Rev. Lett. **121**, 203601 (2018).

[78] H. Y. Yuan, P. Yan, S. Zheng, Q. Y. He, K. Xia, and M.-H. Yung, Phys. Rev. Lett. **124**, 053602 (2020).

[79] T. Nishioka, Rev. Mod. Phys. **90**, 035007 (2018).

[80] R. Islam, R. Ma, P. M. Preiss, M. Eric Tai, A. Lukin, M. Rispoli, and M. Greiner, Nature (London) **528**, 77 (2015).